Inorganic Chemistry

pubs.acs.org/IC

Featured Article

Iridium-Triggered Allylcarbamate Uncaging in Living Cells

Neelu Singh,[†] Ajay Gupta,[†] Puja Prasad, Pritam Mahawar, Shalini Gupta, and Pijus K. Sasmal*

Cite This: *Inorg. Chem.* 2021, 60, 12644−12650

Read Online

ACCESS | Metrics & More | Article Recommendations | Supporting Information

ABSTRACT: Designing a metal catalyst that addresses the major issues of solubility, stability, toxicity, cell uptake, and reactivity within complex biological milieu for bioorthogonal controlled transformation reactions is a highly formidable challenge. Herein, we report an organoiridium complex that is nontoxic and capable of the uncaging of allyloxycarbonyl-protected amines under biologically relevant conditions and within living cells. The potential applications of this uncaging chemistry have been demonstrated by the generation of diagnostic and therapeutic agents upon the activation of profluorophore and prodrug in a controlled fashion within HeLa cells, providing a valuable tool for numerous potential biological and therapeutic applications.

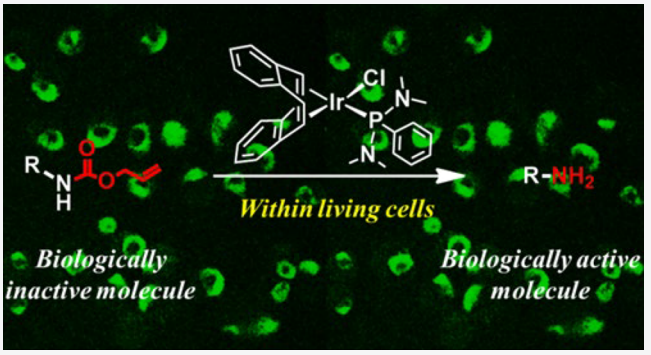

The ability to custom-design synthetic catalysts that can perform artificial chemistry in complex biological milieu has opened up new horizons in medicinal chemistry, chemical biology and the therapeutic treatment of deadly diseases such as cancer. Recently, transition-metal catalysts (TMCs) have emerged as a promising tool for carrying out unnatural chemical transformations via bioorthogonal catalysis in a myriad of cellular environments.[1,2] These chemical transformations have been demonstrated for a variety of applications such as biomolecular labeling,[3] metabolite detection,[4] intracellular probe release,[1,5] and in situ enzyme[6] and prodrug activation.[1b,7] Designing TMC-mediated reactions in living organisms, however, still remains a formidable task for (1) maximization of the catalyst activity at low substrate concentrations, (2) minimization of the catalyst reactivity toward air, water, and other cellular components in high abundance, (3) problems associated with the catalyst toxicity, water solubility, and selectivity toward the desired substrates, and (4) slow uncaging of prodrug for sustained drug release to reduce drug toxicity. Metal-containing catalysts are also often prone to deactivate in the combined presence of air, water, and millimolar concentrations of nucleophilic thiols, raising concerns of their stability in cellular environments.

In the past, researchers have overcome these challenges by developing metal catalysts based on copper-catalyzed azide−alkyne cycloaddition[7d,8] and depropargylation,[9] ruthenium-mediated allylcarbamate cleavage,[1a,5a,b,7b,c,10] redox isomerization,[11] azide reduction[12] and protein labeling,[13] iron-mediated azide reduction,[14] palladium-mediated uncaging of allylcarbamate,[1b,7a,15] propargyloxycarbonyl[5c,6,7a,16] and allenyl groups,[17] etc. In addition, there are cited examples of palladium-mediated N-dealkylation,[7a] O-dealkylation,[18] Suzuki−Miyaura,[1b,3] and Sonogashira cross-couplings,[19] gold-mediated uncaging of a structurally diverse range of functional groups,[7e] propargyl ester amidation,[20] alkyne hydroarylation[21] and hydroamination,[7f] and iridium-catalyzed transfer hydrogenation.[22] While pioneering work on bond cleavage and bond formation reactions was done earlier with copper, iron, ruthenium, palladium, and gold complexes, an important transition metal, iridium, has been unexplored for the same reactions. Like the above-mentioned catalysts, organoiridium complexes can also maintain their catalytic activity in air and biological media[22,23] which makes them suitable for bioorthogonal catalysis reactions inside living cells.

In this study, we report organoiridium(I) complexes for the in situ generation of imaging and therapeutic agents via bioorthogonal allylcarbamate uncaging chemistry in both biological and nonbiological systems without the need of any additives (Figure 1). The uncaging results were demonstrated in protic solvents, phosphate-buffered saline (PBS) buffer, and human cervical cancer (HeLa) cell lysates under air. In addition, the applications of this uncaging chemistry have been displayed by generating diagnostic and therapeutic agents upon the activation of profluorophore and prodrug within HeLa cells.

The organometallic iridium(I) complexes **Ir1**−**Ir3** were developed for the uncaging of *N*-allylcarbamates to their respective amines under biologically relevant conditions and within living cells (Figure 1a). The iridium(I) centers in the synthesized complexes were coordinated with dibenzocyclooc-

Received: June 13, 2021
Published: August 15, 2021

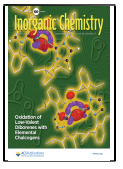

https://doi.org/10.1021/acs.inorgchem.1c01790
Inorg. Chem. 2021, 60, 12644−12650

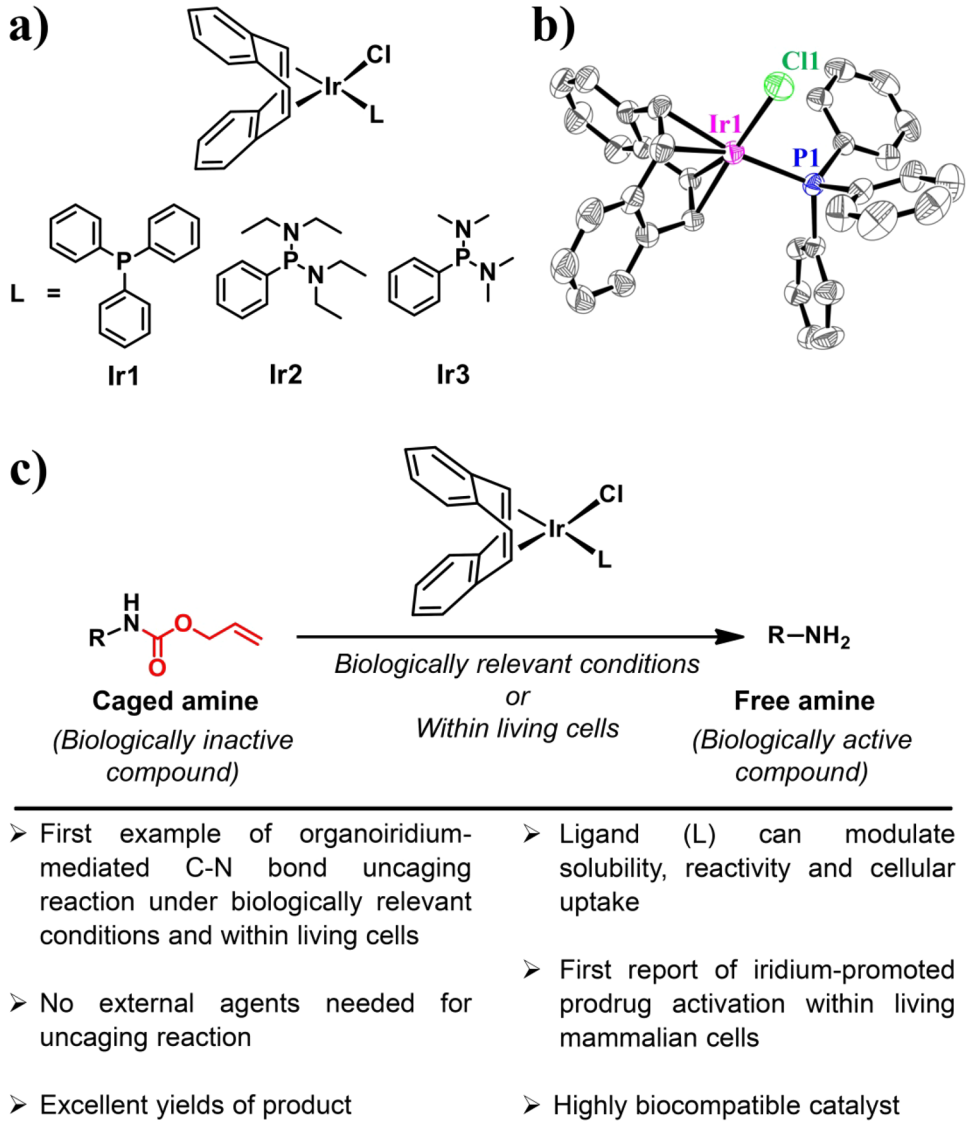

Figure 1. (a) Molecular structures of the iridium(I) complexes (**Ir1**−**Ir3**) used for the uncaging of allylcarbamates in this study. (b) X-ray crystal structure of complex **Ir1**. The hydrogen atoms have been omitted for clarity. (c) Iridium(I)-mediated uncaging of allylcarbamates under biologically relevant conditions or within living cells.

tatetraene (DBCOT) and chloro- and phosphine-based ligands. The iridium(I) center provided a stable square-planar geometry and intracellular uncaging chemistry. The DBCOT ligand was utilized for better cellular uptake due to its hydrophobic nature, which could assist in the effective crossing of the complexes through the lipid bilayers of the cell membranes. In addition, different π-acceptor capabilities of phosphine ligands were coordinated to the metal center to modulate the solubility, reactivity, and cellular uptake of the complexes. In contrast, the chloride ion, an innocent ligand, was added to increase the stability of the complex and to render it ready for direct activation under aqueous environments. The synthesis and characterization data of the ligands and the iridium complexes are described in Schemes S1−S3 and Figures S1−S11. The solid-state structure of **Ir1** was also characterized by X-ray crystallography (Figure 1b and Tables S1 and S2). The stability of the complexes was accessed in organic and aqueous media at room temperature by NMR and absorption spectroscopy (Figures S12 and S13). The complexes exhibit good stability in organic solvents over 72 h but comparatively lower stability in the aqueous medium. The reactivity of iridium complexes due to dissociation of the Ir−Cl bond was investigated by the halide abstraction method (Figure S14).

The synthesized organoiridium complexes (**Ir1**−**Ir3**) were employed for the catalytic deprotection of an allylcarbamate group from a variety of aromatic and aliphatic substrates under air and in the presence of polar protic solvents. For instance, the reaction of *p*-chlorophenyl allylcarbamate (**1a**) with 5 mol % of catalysts **Ir2** and **Ir3** in CH_2Cl_2/MeOH (95:5) at 30 °C under air for 48 h provided isolated yields of *p*-chloroaniline (**1b**) equal to 83 and 76%, respectively (Figure 2). To demonstrate the versatility of these catalysts, we performed the uncaging of allylcarbamates from the electron-rich (**2a** → **2b**) and electron-poor (**3a** → **3b** and **4a** → **4b**) aromatic substrates and found that the catalysis reaction worked efficiently in all cases. Also, these catalysts were utilized for the uncaging of allylcarbamate from the aliphatic amine (**5a** → **5b**) with very good yields. However, **Ir1** worked moderately for the above reactions under the same conditions. The low catalytic activity

https://doi.org/10.1021/acs.inorgchem.1c01790
Inorg. Chem. 2021, 60, 12644−12650

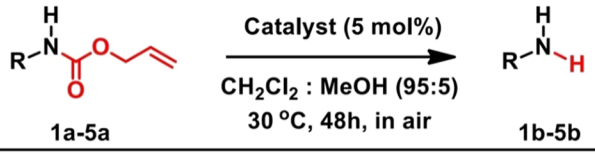

Sl.No.	Substrates	Products	Catalysts	Yield (%)
1	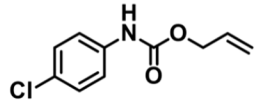 1a	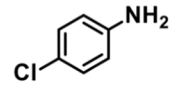 1b	Ir1 Ir2 Ir3	44 83 76
2	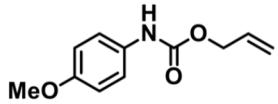 2a	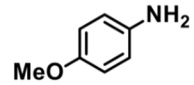 2b	Ir1 Ir2 Ir3	38 92 87
3	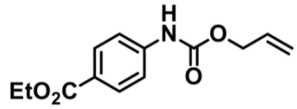 3a	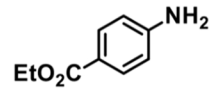 3b	Ir1 Ir2 Ir3	28 87 89
4	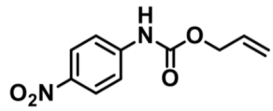 4a	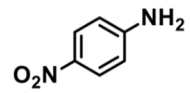 4b	Ir1 Ir2 Ir3	35 63 61
5	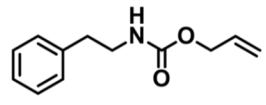 5a	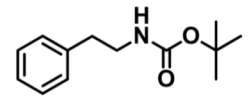 5b	Ir1 Ir2 Ir3	48 90 65

Figure 2. Catalytic deprotection of allylcarbamate-protected amines with organoiridium complexes (**Ir1**−**Ir3**). Reaction conditions: substrate (0.118 mmol, 1 equiv) and catalyst (0.0059 mmol, 0.05 equiv) in 118 μL of CH_2Cl_2/MeOH (95:5, v/v) at 30 °C under air. Shown are the isolated yields of the products.

of **Ir1** was attributed to the bulky structure of its PPh_3 ligand coordinated to the metal center that likely provided steric hindrance toward substrate binding. Notably, no products were isolated in the absence of catalyst. Thus, it was concluded that the organoiridium complexes **Ir2** and **Ir3** smoothly catalyzed the deprotection of allylcarbamates from aromatic and aliphatic amines to their respective amines under mild conditions, without the need of any additives and in the presence of protic solvents and air.

To examine the catalytic activity of organoiridium complexes, we carried out the uncaging of bis(*N*,*N*′-allyloxycarbonyl)rhodamine 110 (**Rho-alloc**) to its corresponding rhodamine 110 (**Rho**) under biologically relevant conditions, which mimicked the native cellular environment. The reactions were carried out either in PBS with trace amounts of glutathione (GSH) or in HeLa cell lysates in the presence of air. The progress of the reaction was simply checked by monitoring the fluorescence readout of the released **Rho**. The best results were obtained with **Ir3** (20 mol %) in which the incubation of nonfluorescent caged rhodamine (**Rho-alloc**, 500 μM) in the presence of GSH (5 mM) in dimethyl sulfoxide (DMSO)/PBS (1:1, 10 mM, pH 7.4) at 37 °C led to a gradual increase in the fluorescence intensity (Figure 3a). The signal reached saturation around 48 h, giving a **Rho** yield of 32 ± 0.8%. In contrast, negative control experiments performed in the absence of an iridium complex showed no fluorescence signal (0.1 ± 0.1%).

When the above experiments were repeated in the presence of HeLa cell lysates, a more complex and biologically realistic environment, the iridium-promoted reactions still showed great response albeit with slightly lower yields. The yield was 11 ± 0.5% after 48 h and continued to rise even up to the fourth day, before gradually leveling off at 16 ± 0.5% (Figure S15). When similar experiments were, however, repeated with complexes **Ir1** and **Ir2** either in PBS or HeLa cell lysates, **Ir2** gave only ∼6.5 ± 0.6% yield of **Rho**, while **Ir1** was found to be almost inactive (ca. ∼1.5% yield) after 48 h.

In general, the yield of **Rho** in PBS or cell lysates was lower compared to the yield of uncaged amine (**1b**−**5b**) in CH_2Cl_2/MeOH. The reason for this lower yield of **Rho** under biorelevant conditions might be associated with the slow deactivation of catalyst (Figure S13). Besides, **Ir1** was found to be inactive, which may possibly be due to its low solubility in an aqueous medium because of the hydrophobic PPh_3 ligand[15b] and, in addition, to its bulky structure, which can cause steric crowding toward substrate binding.

Further, we investigated the catalytic uncaging of allylcarbamate from the prodrug of doxorubicin (DOX), a well-known

https://doi.org/10.1021/acs.inorgchem.1c01790
Inorg. Chem. 2021, 60, 12644−12650

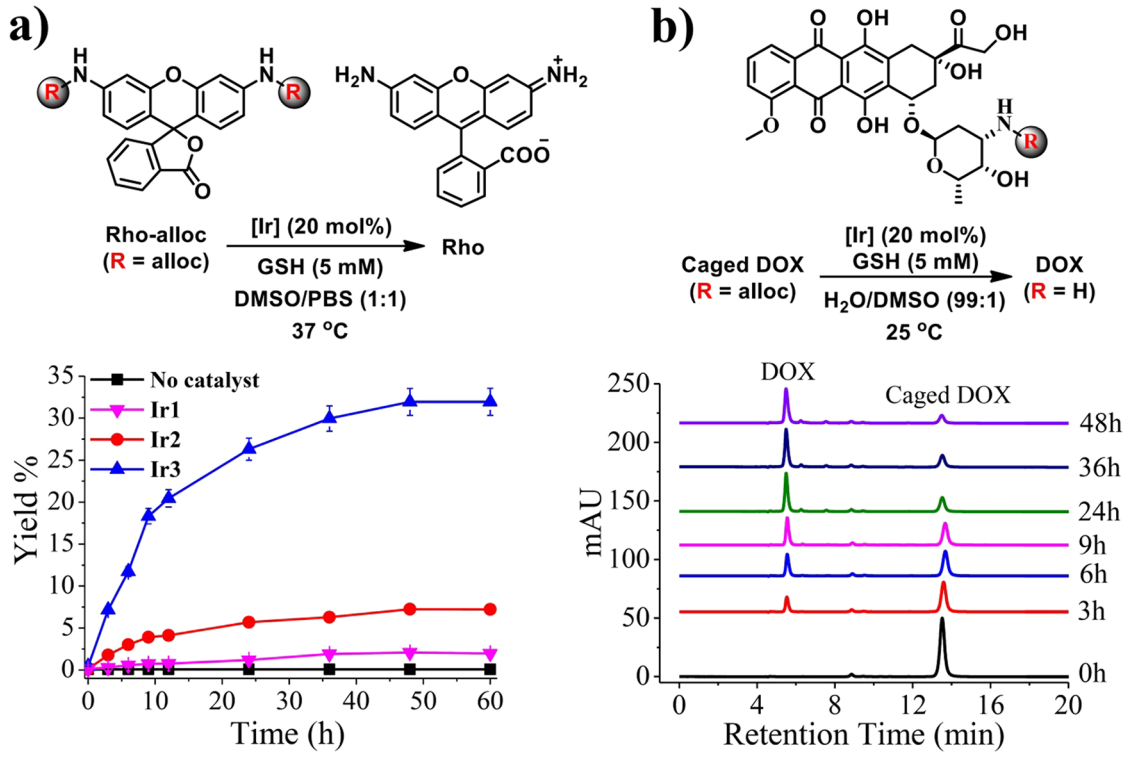

Figure 3. (a) Uncaging of **Rho-alloc** (0.5 mM, 1 equiv) mediated by an organoiridium complex (0.1 mM, 0.2 equiv) in DMSO/PBS (1:1, v/v) at 37 °C in the presence of GSH (5 mM, 10 equiv). Yields were determined by comparing the fluorescence intensities (λ_{ex} = 488 nm; λ_{em} = 520 nm) of diluted samples with a standard curve of different concentrations of **Rho**. (b) Catalytic uncaging of caged DOX (100 μM) with **Ir3** (20 μM) and GSH (5 mM) in water/DMSO (99:1) at 25 °C monitored by HPLC.

chemotherapeutic anticancer drug used in the treatment of a wide range of cancers. For this purpose, the allylcarbamate-protected doxorubicin prodrug (caged DOX, 100 μM) was incubated with 20 μM **Ir2** or **Ir3** and 5 mM GSH in water/DMSO (99:1) at room temperature under air. The deprotection of allylcarbamate was monitored for 48 h, and the results were analyzed using analytical high-performance liquid chromatography (HPLC; Figures 3b and S16 and S17). The results showed that the loading of 20 mol % **Ir2** and **Ir3** to caged DOX gave 29% and 76% DOX release, respectively. As expected, the yield decreased upon reduction of the catalyst loading, and there was no product formation in the absence of the catalyst. This clearly proved that the catalyst was able to activate the prodrug in the extracellular medium. On the basis of these observations, we tentatively proposed an iridium-triggered allylcarbamate uncaging pathway (Figure S18).

Next, we carried out iridium-triggered artificial chemistry for allylcarbamate uncaging within the highly complex biological milieu for translation to cellular habitats. For this, cultured HeLa cells were incubated with caged rhodamine (**Rho-alloc**, 100 μM) for 30 min, followed by multiple washings with PBS to remove the caged fluorophore from the extracellular solution and to ensure that **Rho-alloc** is located only within the HeLa cells, not in the culture medium. A fresh medium was added to the cells along with **Ir3** (20 μM), which led to the development of cellular green fluorescence, indicating the formation of **Rho** (Figures 4a and S19 and S20). The development of green fluorescence intensity was monitored by live-cell confocal microscopy imaging, and the results revealed a 56-fold increase in the fluorescence intensity within HeLa cells over a period of 8 h. In contrast, the cells treated with the caged substrate in the absence of catalyst were found to be nonfluorescent. These results indicated the successful uncaging of allylcarbamate from **Rho-alloc** by the catalyst within live HeLa cells and the subsequent release of fluorescent **Rho**. More notably, the catalyst showed a high efficiency, as determined by the significant increase in the fluorescence intensity, and long periods of activity suggest its slow deactivation in complex biological environments.

To further determine the accumulation of catalyst at the subcellular level, we carried out inductively coupled plasma mass spectrometry (ICP-MS; Figure S21). The ICP-MS data showed a high accumulation of iridium inside the cell cytosol, suggesting that allylcarbamate cleavage from caged rhodamine (**Rho-alloc**) by **Ir3** mostly occurred within the cytoplasm, followed by slow diffusion of the green fluorescent product (**Rho**) throughout the cells. We also determined the tolerance of cells in the presence of catalyst before proceeding to prodrug activation. Our cell viability results revealed the catalyst to be nontoxic (ca. >96% viable cells) at 50 μM concentration even after a long incubation period of 48 h, as determined by MTT assay (Figure 4b).

The ability to activate profluorophore by a catalyst within living cells and its high biocompatibility motivated us to study the bioorthogonal activation of a prodrug inside cells. Moreover, the slow uncaging of allylcarbamate by **Ir3** in the biological medium can be advantageous for the activation of prodrug for sustained drug release. The sustained release of drug is highly beneficial over the burst release because the latter can cause dangerous spikes in drug concentrations, resulting undesirable side effects. Hence, we demonstrated the bioorthogonal catalytic activation of a prodrug to establish our proof-of-concept. For this, we utilized our previously synthesized caged DOX, which was converted to DOX upon

https://doi.org/10.1021/acs.inorgchem.1c01790
Inorg. Chem. 2021, 60, 12644−12650

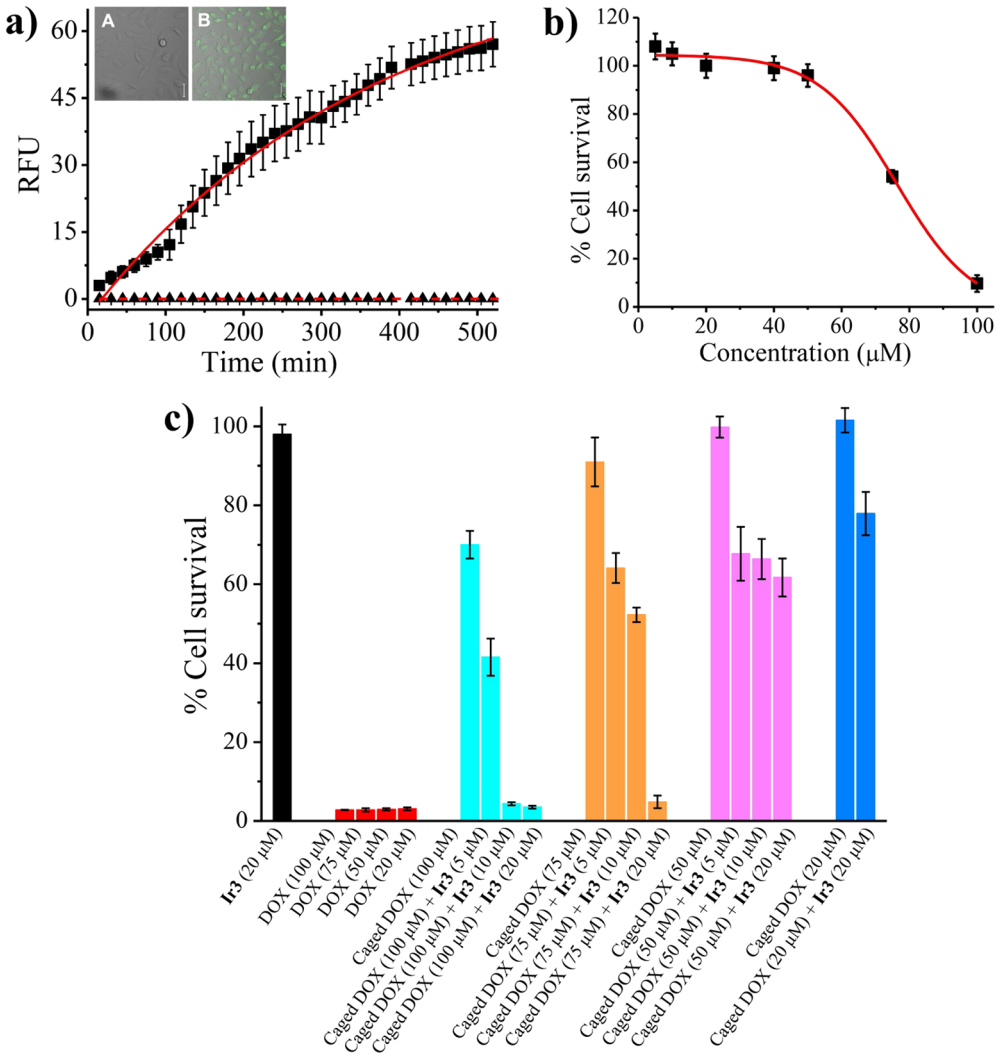

Figure 4. (a) Uncaging of **Rho-alloc** (100 μM) with (■) and without (▲) addition of **Ir3** (20 μM) in HeLa cells monitored by live-cell imaging using confocal microscopy. Insets: (A) bright-field image of cells treated with **Rho-alloc** only (control) and (B) merged bright-field image of cells treated with **Rho-alloc** and **Ir3**. Both images were taken after 8 h. Scale bar: 10 μm. (b) Cytotoxicity of **Ir3** in HeLa cells after 48 h of incubation (IC_{50} = 76 μM) as determined by MTT assay. (c) Activation of a prodrug (caged DOX) by **Ir3** inside HeLa cells. The cell survival rates were determined by MTT assay.

catalytic uncaging of the allylcarbamate group. We determined the cell viability of caged DOX in the presence of an iridium complex in HeLa cells by MTT assay (Figures 4c and S22 and S23). The HeLa cells were incubated with different concentrations of caged DOX (20, 50, 75, and 100 μM) for 3 h, followed by incubation with an iridium complex (20 μM) in a fresh medium for 48 h. Not surprisingly, the caged DOX was found to be nontoxic to the cells in the absence of catalyst, whereas the free drug DOX showed toxicity. We observed only a small decrease in the cell viability when 20 μM caged DOX was incubated with 20 μM catalyst for 48 h. However, when the concentration of nontoxic caged DOX was increased from 20 to 100 μM while the catalyst concentration was kept fixed at 20 μM, the cell viability decreased drastically in a concentration-dependent manner. Interestingly, we could observe efficient reduction of the cell viability even with a decreased catalyst loading of 10 or 5 μM in the presence of a high concentration of caged DOX (100 μM). This drastic decrease in the cell viability with the prodrug in the presence of a catalyst suggests uncaging of the allylcarbamate group inside the cells.

In conclusion, we have reported three organometallic iridium(I) complexes (**Ir1**−**Ir3**) for catalytic deprotection of allylcarbamate-protected amines in biological and nonbiological conditions without the need of any exogenous agents. The catalysts **Ir2** and **Ir3** efficiently performed the uncaging of allylcarbamate from a variety of aromatic and aliphatic substrates in the presence of protic solvents and air. The uncaging results with profluorophore and prodrug under biologically relevant conditions showed good efficiency, with the best performance obtained with the catalyst **Ir3**. The catalyst **Ir3** also exhibited a remarkably high activity, with up to a 56-fold increase in the fluorescence intensity over a period of 8 h for the uncaging of allylcarbamate from profluorophore within live HeLa cells. In addition, activation of the prodrug by the catalyst **Ir3** inside HeLa cells provided both prodrug and catalyst concentration-dependent cell death. In the future, the prodrug and profluorophore systems could be suitably combined to allow the real-time tracking of cell death.

https://doi.org/10.1021/acs.inorgchem.1c01790
Inorg. Chem. 2021, 60, 12644−12650

■ ASSOCIATED CONTENT

Supporting Information

The Supporting Information is available free of charge at https://pubs.acs.org/doi/10.1021/acs.inorgchem.1c01790.

Materials and methods, experimental details, syntheses, characterization, single-crystal X-ray diffraction, biological studies, and figures and tables (PDF)

Accession Codes

CCDC 2052132 contains the supplementary crystallographic data for this paper. These data can be obtained free of charge via www.ccdc.cam.ac.uk/data_request/cif, or by emailing data_request@ccdc.cam.ac.uk, or by contacting The Cambridge Crystallographic Data Centre, 12 Union Road, Cambridge CB2 1EZ, UK; fax: +44 1223 336033.

■ AUTHOR INFORMATION

Corresponding Author

Pijus K. Sasmal − *School of Physical Sciences, Jawaharlal Nehru University (JNU), New Delhi 110067, India;* orcid.org/0000-0002-2301-1269; Email: pijus@mail.jnu.ac.in

Authors

Neelu Singh − *School of Physical Sciences, Jawaharlal Nehru University (JNU), New Delhi 110067, India*

Ajay Gupta − *School of Physical Sciences, Jawaharlal Nehru University (JNU), New Delhi 110067, India*

Puja Prasad − *Department of Chemical Engineering, Indian Institute of Technology (IIT) Delhi, New Delhi 110016, India*

Pritam Mahawar − *Department of Chemistry, Indian Institute of Technology (IIT) Delhi, New Delhi 110016, India*

Shalini Gupta − *Department of Chemical Engineering, Indian Institute of Technology (IIT) Delhi, New Delhi 110016, India;* orcid.org/0000-0003-1382-0254

Complete contact information is available at: https://pubs.acs.org/10.1021/acs.inorgchem.1c01790

Author Contributions

†N.S. and A.G. contributed equally to this work.

Notes

The authors declare no competing financial interest.

■ ACKNOWLEDGMENTS

P.K.S. acknowledges SERB, DST (Grant no. ECR/2016/000810), and DST-PURSE for financial assistance. S.G. acknowledges funding received from DST Nanomission (Grant no. SR/NM/NT-1049/2016) and IMPRINT (Grant no. IMP/2018/000236/HT). We thank DST-FIST for Single Crystal X-ray Diffraction facility in SPS, JNU, and AIRF, JNU for the instrumentation facilities. N.S. gratefully acknowledges SERB, DST, for a junior research fellowship. A.G. acknowledges MHRD-STARS for a fellowship. P.P. thanks CSIR for the SRA position (Pool No. 9031-A). We thank Dr. D. Das and L. Negi, SPS, JNU, for help with X-ray data collection and for solving the crystal structure of **Ir1**. We sincerely thank Prof. S. Nagendran, IIT Delhi, for allowing us to use his glovebox for the synthesis of an iridium-dimer precursor. R. K. Sah, SCMM, JNU, is gratefully acknowledged for live-cell imaging data collection. We thank Prof. E. Meggers, Philipps Universitat Marburg, Marburg, Germany, for helpful discussions and his input and comments on this manuscript.

■ REFERENCES

(1) (a) Streu, C.; Meggers, E. Ruthenium-induced allylcarbamate cleavage in living cells. *Angew. Chem., Int. Ed.* **2006**, *45*, 5645−5648. (b) Yusop, R. M.; Unciti-Broceta, A.; Johansson, E. M. V.; Sánchez-Martín, R. M.; Bradley, M. Palladium-mediated intracellular chemistry. *Nat. Chem.* **2011**, *3*, 239−243.

(2) (a) Sasmal, P. K.; Streu, C. N.; Meggers, E. Metal complex catalysis in living biological systems. *Chem. Commun.* **2013**, *49*, 1581−1587. (b) Bai, Y.; Chen, J.; Zimmerman, S. C. Designed transition metal catalysts for intracellular organic synthesis. *Chem. Soc. Rev.* **2018**, *47*, 1811−1821. (c) Rebelein, J. G.; Ward, T. R. *In vivo* catalyzed new-to-nature reactions. *Curr. Opin. Biotechnol.* **2018**, *53*, 106−114. (d) Ngo, A. H.; Bose, S.; Do, L. H. Intracellular chemistry: Integrating molecular inorganic catalysts with living systems. *Chem. - Eur. J.* **2018**, *24*, 10584−10594. (e) Martínez-Calvo, M.; Mascareñas, J. L. Organometallic catalysis in biological media and living settings. *Coord. Chem. Rev.* **2018**, *359*, 57−79. (f) Zhang, X.; Huang, R.; Gopalakrishnan, S.; Cao-Milán, R.; Rotello, V. M. Bioorthogonal Nanozymes: Progress towards Therapeutic Applications. *Trends Chem.* **2019**, *1*, 90−98. (g) Liu, Y.; Bai, Y. Design and engineering of metal catalysts for bio-orthogonal catalysis in living systems. *ACS Appl. Bio Mater.* **2020**, *3*, 4717−4746. (h) van de L'Isle, M. O. N.; Ortega-Liebana, M. C.; Unciti-Broceta, A. *Curr. Opin. Chem. Biol.* **2021**, *61*, 32−42. (i) Destito, P.; Vidal, C.; López, F.; Mascareñas, J. L. Transition metal-promoted reactions in aqueous media and biological settings. *Chem. - Eur. J.* **2021**, *27*, 4789−4816. (j) Nguyen, D. P.; Nguyen, H. T. H.; Do, L. H. Tools and methods for investigating synthetic metal-catalyzed reactions in living cells. *ACS Catal.* **2021**, *11*, 5148−5165.

(3) Spicer, C. D.; Triemer, T.; Davis, B. G. Palladium-mediated cell-surface labeling. *J. Am. Chem. Soc.* **2012**, *134*, 800−803.

(4) Michel, B. W.; Lippert, A. R.; Chang, C. J. A reaction-based fluorescent probe for selective imaging of carbon monoxide in living cells using a palladium-mediated carbonylation. *J. Am. Chem. Soc.* **2012**, *134*, 15668−15671.

(5) (a) Sasmal, P. K.; Carregal-Romero, S.; Parak, W. J.; Meggers, E. Light-triggered ruthenium-catalyzed allylcarbamate cleavage in biological environments. *Organometallics* **2012**, *31*, 5968−5970. (b) Hsu, H.-T.; Trantow, B. M.; Waymouth, R. M.; Wender, P. A. Bioorthogonal catalysis: A general method to evaluate metal-catalyzed reactions in real time in living systems using a cellular luciferase reporter system. *Bioconjugate Chem.* **2016**, *27*, 376−382. (c) Indrigo, E.; Clavadetscher, J.; Chankeshwara, S. V.; Megia-Fernandez, A.; Lilienkampf, A.; Bradley, M. Intracellular delivery of a catalytic organometallic complex. *Chem. Commun.* **2017**, *53*, 6712−6715.

(6) Li, J.; Yu, J.; Zhao, J.; Wang, J.; Zheng, S.; Lin, S.; Chen, L.; Yang, M.; Jia, S.; Zhang, X.; Chen, P. R. Palladium-triggered deprotection chemistry for protein activation in living cells. *Nat. Chem.* **2014**, *6*, 352−361.

(7) (a) Weiss, J. T.; Dawson, J. C.; Macleod, K. G.; Rybski, W.; Fraser, C.; Torres-Sánchez, C.; Patton, E. E.; Bradley, M.; Carragher, N. O.; Unciti-Broceta, A. Extracellular palladium-catalyzed dealkylation of 5-fluoro-1-propargyl-uracil as a bioorthogonally activated prodrug approach. *Nat. Commun.* **2014**, *5*, 3277−3285. (b) Volker, T.; Dempwolff, F.; Graumann, P. L.; Meggers, E. Progress towards bioorthogonal catalysis with organometallic compounds. *Angew. Chem., Int. Ed.* **2014**, *53*, 10536−10540. (c) Tonga, G. Y.; Jeong, Y.; Duncan, B.; Mizuhara, T.; Mout, R.; Das, R.; Kim, S. T.; Yeh, Y.-C.; Yan, B.; Hou, S.; Rotello, V. M. Supramolecular regulation of bioorthogonal catalysis in cells using nanoparticle-embedded transition metal catalysts. *Nat. Chem.* **2015**, *7*, 597−603. (d) Clavadetscher, J.; Hoffmann, S.; Lilienkampf, A.; Mackay, L.; Yusop, R. M.; Rider, S. A.; Mullins, J. J.; Bradley, M. Copper catalysis in living systems and in situ drug synthesis. *Angew. Chem., Int. Ed.* **2016**, *55*, 15662−15666. (e) Pérez-López, A. M.; Rubio-Ruiz, B.; Sebastian, V.; Hamilton, L.; Adam, C.; Bray, T. L.; Irusta, S.; Brennan, P. M.; Lloyd-

Jones, G. C.; Sieger, D.; Santamaria, J.; Unciti-Broceta, A. Gold-triggered uncaging chemistry in living systems. *Angew. Chem., Int. Ed.* **2017**, *56*, 12548−12552. (f) Chang, T.-S.; Vong, K.; Yamamoto, T.; Tanaka, K. Prodrug activation by gold artificial metalloenzyme-catalyzed synthesis of phenanthridinium derivatives via hydro-amination. *Angew. Chem., Int. Ed.* **2021**, *60*, 12446−12454.

(8) (a) Wang, F.; Zhang, Y.; Liu, Z.; Du, Z.; Zhang, L.; Ren, J.; Qu, X. A biocompatible heterogeneous MOF-Cu catalyst for in vivo drug synthesis in targeted subcellular organelles. *Angew. Chem., Int. Ed.* **2019**, *58*, 6987−6992. (b) Bai, Y.; Feng, X.; Xing, H.; Xu, Y.; Kim, B. K.; Baig, N.; Zhou, T.; Gewirth, A. A.; Lu, Y.; Oldfield, E.; Zimmerman, S. C. A Highly efficient single-chain metal-organic nanoparticle catalyst for alkyne-azide "click" reactions in water and in cells. *J. Am. Chem. Soc.* **2016**, *138*, 11077−11080.

(9) Liu, Y.; Pujals, S.; Stals, P. J. M.; Paulöhrl, T.; Presolski, S. I.; Meijer, E. W.; Albertazzi, L.; Palmans, A. R. A. Catalytically active single-chain polymeric nanoparticles: Exploring their functions in complex biological media. *J. Am. Chem. Soc.* **2018**, *140*, 3423−3433.

(10) (a) Tomás-Gamasa, M.; Martínez-Calvo, M.; Couceiro, J. R.; Mascareñas, J. L. Transition metal catalysis in the mitochondria of living cells. *Nat. Commun.* **2016**, *7*, 12538. (b) Zhang, X.; Liu, Y.; Gopalakrishnan, S.; Castellanos-Garcia, L.; Li, G.; Malassiné, M.; Uddin, I.; Huang, R.; Luther, D. C.; Vachet, R. W.; Rotello, V. M. Intracellular activation of bioorthogonal nanozymes through endosomal proteolysis of the protein corona. *ACS Nano* **2020**, *14*, 4767−4773.

(11) Vidal, C.; Tomás-Gamasa, M.; Gutiérrez-González, A.; Mascareñas, J. L. Ruthenium-catalyzed redox isomerizations inside Living Cells. *J. Am. Chem. Soc.* **2019**, *141*, 5125−5129.

(12) Chen, J.; Li, K.; Shon, J. S. L.; Zimmerman, S. C. Single-chain nanoparticle delivers a partner enzyme for concurrent and tandem catalysis in cells. *J. Am. Chem. Soc.* **2020**, *142*, 4565−4569.

(13) Sadhu, K. K.; Lindberg, E.; Winssinger, N. In cellulo protein labelling with Ru-conjugate for luminescence imaging and bio-orthogonal photocatalysis. *Chem. Commun.* **2015**, *51*, 16664−16666.

(14) (a) Sasmal, P. K.; Carregal-Romero, S.; Han, A. A.; Streu, C. N.; Lin, Z.; Namikawa, K.; Elliott, S. L.; Köster, R. W.; Parak, W. J.; Meggers, E. Catalytic azide reduction in biological environments. *ChemBioChem* **2012**, *13*, 1116−1120. (b) Huang, R.; Li, C. H.; Cao-Milan, R.; He, L. D.; Makabenta, J. M.; Zhang, X. Z.; Yu, E. L.; Rotello, V. M. Polymer-based bioorthogonal nanocatalysts for the treatment of bacterial biofilms. *J. Am. Chem. Soc.* **2020**, *142*, 10723−10729.

(15) (a) Wang, F.; Zhang, Y.; Du, Z.; Ren, J.; Qu, X. Designed heterogeneous palladium catalysts for reversible light-controlled bioorthogonal catalysis in living cells. *Nat. Commun.* **2018**, *9*, 1209. (b) Martínez-Calvo, M.; Couceiro, J. R.; Destito, P.; Rodríguez, J.; Mosquera, J.; Mascareñas, J. L. Intracellular deprotection reactions mediated by palladium complexes equipped with designed phosphine ligands. *ACS Catal.* **2018**, *8*, 6055−6061.

(16) (a) Pérez-López, A. M.; Rubio-Ruiz, B.; Valero, T.; Contreras-Montoya, R.; Álvarez De Cienfuegos, L.; Sebastián, V.; Santamaría, J.; Unciti-Broceta, A. Bioorthogonal uncaging of cytotoxic paclitaxel through Pd nanosheet-hydrogel frameworks. *J. Med. Chem.* **2020**, *63*, 9650−9659. (b) Learte-Aymamí, S.; Vidal, C.; Gutiérrez-González, A.; Mascareñas, J. L. Intracellular reactions promoted by bis-(histidine) miniproteins stapled using palladium(II) complexes. *Angew. Chem., Int. Ed.* **2020**, *59*, 9149−9154.

(17) Wang, J.; Zheng, S.; Liu, Y.; Zhang, Z.; Lin, Z.; Li, J.; Zhang, G.; Wang, X.; Li, J.; Chen, P. R. Palladium-triggered chemical rescue of intracellular proteins via genetically encoded allene-caged tyrosine. *J. Am. Chem. Soc.* **2016**, *138*, 15118−15121.

(18) Sancho-Albero, M.; Rubio-Ruiz, B.; Pérez-López, A. M.; Sebastián, V.; Martín-Duque, P.; Arruebo, M.; Santamaría, J.; Unciti-Broceta, A. Cancer-derived exosomes loaded with ultrathin palladium nanosheets for targeted bioorthogonal catalysis. *Nat. Catal.* **2019**, *2*, 864−872.

(19) Li, J.; Lin, S. X.; Wang, J.; Jia, S.; Yang, M. Y.; Hao, Z. Y.; Zhang, X. Y.; Chen, P. R. Ligand-free palladium-mediated site-specific protein labeling inside gram-negative bacterial pathogens. *J. Am. Chem. Soc.* **2013**, *135*, 7330−7338.

(20) Tsubokura, K.; Vong, K. K.; Pradipta, A. R.; Ogura, A.; Urano, S.; Tahara, T.; Nozaki, S.; Onoe, H.; Nakao, Y.; Sibgatullina, R.; Kurbangalieva, A.; Watanabe, Y.; Tanaka, K. In vivo gold complex catalysis within live mice. *Angew. Chem., Int. Ed.* **2017**, *56*, 3579−3584.

(21) Vidal, C.; Tomás-Gamasa, M.; Destito, P.; López, F.; Mascareñas, J. L. Concurrent and orthogonal gold(I) and ruthenium-(II) catalysis inside living cells. *Nat. Commun.* **2018**, *9*, 1913 DOI: 10.1038/s41467-018-04314-5.

(22) Bose, S.; Ngo, A. H.; Do, L. H. Intracellular transfer hydrogenation mediated by unprotected organoiridium catalysts. *J. Am. Chem. Soc.* **2017**, *139*, 8792−8795.

(23) (a) Song, W.; Zheng, N. Iridium-catalyzed highly regioselective azide−ynamide cycloaddition to access 5-amido fully substituted 1,2,3-triazoles under mild, air, aqueous, and bioorthogonal conditions. *Org. Lett.* **2017**, *19*, 6200−6203. (b) Chen, R.; Zeng, L.; Lai, Z.; Cui, S. Iridium-catalyzed hydroxyl-enabled cycloaddition of azides and alkynes. *Adv. Synth. Catal.* **2019**, *361*, 989−994.

https://doi.org/10.1021/acs.inorgchem.1c01790
Inorg. Chem. 2021, 60, 12644−12650